minerals

MDPI

Article

Stability of CO_2 Fluid in Eclogitic Mantle Lithosphere: Thermodynamic Calculations

Yulia G. Vinogradova and Anton Shatskiy *

Vernadsky Institute of Geochemistry and Analytical Chemistry, Russian Academy of Science, Moscow 119991, Russia; vinogradova@geokhi.ru

* Correspondence: shatskiyantonf@gmail.com or shatskiy@geokhi.ru; Tel.: +7-(913)-385-61-29

Abstract: Findings of solid and liquefied CO_2 in diamonds from kimberlites and placers have indicated its presence in the form of a fluid phase in the Earth's mantle at depths of 150–250 km. However, this is inconsistent with the results of experiments and existing thermodynamic calculations. To clarify this, we carried out thermodynamic modeling of garnet–CO_2 and bimineral eclogite–CO_2 systems using the Perple_X v. 7.1.3 software package, which establishes the most thermodynamically favorable assemblages for a given bulk composition of the system, unlike previous calculations, for which the phase relationships were simply assumed. The key difference between our results and previously known data is the presence of a region of partial carbonation. In this region, the garnet and clinopyroxene of the new compositions, CO_2 fluid, carbonates, kyanite, and coesite are in equilibrium. The calculations revealed that unlike endmember systems (pyrope–CO_2 and diopside–CO_2) in the eclogite–CO_2 system, the carbonation and decarbonation lines do not coincide, and the Grt+Cpx+CO_2 and Carb+Ky+Coe+Cpx fields are separated by the Grt+Cpx+CO_2+Carb+Ky+Coe region, which extends to pressures exceeding 4.3–6.0 GPa at 1050–1200 °C. This should extend the CO_2 stability field in the eclogitic mantle to lower temperatures. Yet, owing to the short CO_2 supply in the real mantle, the CO_2 fluid should be completely spent on the carbonation of eclogite just below the eclogite + CO_2 field. Thus, according to the obtained results, the CO_2 fluid is stable in the eclogitic mantle in the diamond stability field at temperatures exceeding 1250 °C and pressures of 5–6 GPa.

Keywords: CO_2 fluid; Earth's mantle; phase relations; thermodynamic calculations

Citation: Vinogradova, Y.G.; Shatskiy, A. Stability of CO_2 Fluid in Eclogitic Mantle Lithosphere: Thermodynamic Calculations. *Minerals* **2024**, *14*, 403. https://doi.org/10.3390/min14040403

Received: 3 February 2024
Revised: 22 March 2024
Accepted: 13 April 2024
Published: 15 April 2024

1. Introduction

CO_2 is an important volatile component responsible for the partial melting and generation of magmas such as kimberlites and carbonatites in the Earth's upper mantle [1]. Unlike subducted H_2O/OH^-, which is mostly lost at subarc depths [2–4], CO_2 as carbonates sinks deeper into the mantle [5] and is extracted in the form of a carbonate melt [6] or CO_2 fluid during the progressive warming of a stagnant slab [7]. Findings of inclusions saturated with volatile components in the eclogites of the diamond facies of metamorphism are rare, and all of them are confined to diamond crystals. Shatsky et al. [8] reported numerous $CaCO_3$ microinclusions in diamonds from an eclogite xenolith from the Udachnaya pipe (Russia). Zedgenizov et al. [9] described findings of K-rich low-Mg chloride–carbonate microinclusions in diamonds with a fibrous internal structure from an eclogite xenolith of the same pipe.

Considering the findings of liquefied CO_2 in minerals associated with the diamond deposits reported by Roedder [10], Kennedy and Nordlie [11] suggested that CO_2 was responsible for the diamonds' formation. Later, CO_2 inclusions were indeed discovered in the diamonds themselves. These were submicron solid inclusions under residual levels of pressure up to 5 GPa [12–14] and optically visible (10–70 μm) liquid inclusions in healed fractures mixed with N_2 and hydrocarbons [15,16]. The findings of these inclusions may indicate the presence of CO_2 fluid in the crystallization medium of some diamonds.

Furthermore, the crystallization of diamonds in CO_2 fluid was realized in experiments under *P-T* conditions close to those for natural diamond formation [17]. However, according to experimental data, the stability of CO_2 in the most common ultramafic mantle is limited by carbonation reactions involving olivine, which occur at pressures of 1.0–2.5 GPa [18,19].

It should also be noted that mineral inclusions found in CO_2-bearing diamonds belong to the eclogitic suite [13,20,21]. Meanwhile, some diamonds that entrapped solid CO_2 at higher pressures may have formed under different conditions—such as based on the redox freezing mechanism [22]. Experiments show that the stability field of CO_2 fluid with minerals of the eclogitic suite in the pyrope–CO_2 and diopside–CO_2 systems extends to higher pressures compared to the peridotite mantle but still does not reach the diamond stability field [23–27]. Nevertheless, the studied systems do not adequately model the compositions of eclogite garnets and clinopyroxenes, which are known to be represented by pyrope–almandine–grossular solid solutions and omphacite (diopside–jadeite solid solution), respectively. Using thermodynamic calculations, Knoche et al. [23] showed that the dilution of the diopside component in clinopyroxene and the pyrope component in garnet shifts the carbonation reaction boundaries to higher pressures. These calculations were verified by experiments with clinopyroxenes of the diopside–jadeite series [28]. The results showed that jadeite does not undergo a carbonation reaction, so clinopyroxene with a high jadeite content coexists with CO_2 to at least 6–6.5 GPa and 1050–1100 °C. In the case of garnet, experimentally identified trends are not so obvious. The stability field of the Grt+CO_2 assemblage in the $Prp_{35}Alm_{40}Grs_{25}$–CO_2 system extends to lower temperatures relative to those of the Prp–CO_2 system at a pressure of 3 GPa but remains unchanged at 6.3 and 7.5 GPa [29]. A similar trend is observed in the $Prp_{30}Alm_{70}$–CO_2 system [25].

Previous thermodynamic calculations [23,25,30] assume that regardless of the composition of the solid solution outside the Grt+CO_2 field, garnet completely reacts with CO_2 to produce kyanite, coesite, and carbonate as shown below:

$$(Ca,Mg,Fe)_3Al_2Si_3O_4\ (Prp) + 3CO_2\ (fluid) = 3(Ca,Mg,Fe)CO_3\ (Carb) + Al_2SiO_5\ (Ky) + 2SiO_2\ (Qz/Coe). \quad (1)$$

Yet, the experiments reveal the garnet crystallization outside the Grt+CO_2 stability field, wherein the cation composition of the newly formed garnet differs significantly from the bulk composition of the Grt–CO_2 system [25,29,31]. These may be associated either with sluggish kinetics or more complex phase relations.

To clarify this in the present study, we carried out thermodynamic modeling of the pyrope–almandine–grossular–CO_2 system using the Perple_X v. 7.1.3 software package [32,33], which establishes the most thermodynamically favorable assemblage for a given bulk composition of a system, unlike previous calculations, in which the phase relationships were simply assumed. Finally, we also performed thermodynamic calculations for the bimineral eclogite–CO_2 system.

2. Methods

T-X diagrams and *P-T* pseudo-sections were calculated using the Perple_X v. 7.1.3 software package [32] in the range of 900–1500 °C and 3–6 GPa. The calculations were carried out for the CaO-MgO-FeO-Al_2O_3-SiO_2-CO_2 system (+Na_2O when modeling eclogite) with component ratios corresponding to reagents in carbonation reactions taken in equal proportions (i.e., Grt+3CO_2 and Cpx+2CO_2). The calculations were performed for the following subsystems: (1) Prp–Grs+CO_2, (2) Prp–$Alm_{50}Grs_{50}$+CO_2, and $Prp_{50}Grs_{25}Alm_{25}$+$Di_{70}Jd_{30}$+5CO_2. For the mineral component, the database from Holland and Powell [34] was used with compatible solution models: the Gt(HGP) model for garnet (pyrope-grossular-almandine) [35]; Omph(HP) for a clinopyroxene (diopside-jadeite-hedenbergite-Ca-tschermak) [11,36], oCcM(EF) for a ternary solution of calcite–magnesite–siderite, and LIQ(EF) for a carbonate melt [37]. For CO_2 fluid, we use compensated Redlich–Kwong (CORK) EOS from Holland and Powell [38] who extended the modified Redlich–Kwong (MRK) EOS to 5 GPa and 1600 °C. Calculations were performed with the default resolution values since they did not cause significant distortions in the diagrams. Minimization was conducted on a 4-level grid with 40 × 40 nodes, which had a

spacing of 9.6 MPa (0.0096 GPa) at 1.9 °C and 0.3 mol%. The equations of states of a ternary solution of calcite–magnesite–siderite carbonates oCcM(EF) and a carbonate melt LIQ(EF) are both based on the experiments at 3.5 GPa in $CaCO_3$-$MgCO_3$-$FeCO_3$ system [37].

The solid solution models for garnet and clinopyroxene were chosen based on the results of studies on phase relations along the pyrope–grossular join [39–43]. The existence of a miscibility gap was reported in all studies, though its position varies. Immiscibility is accompanied by the formation of clinopyroxene with the diopside–Ca–tschermak composition, which corresponds to the $CaSiO_3$-$MgSiO_3$-Al_2O_3 ternary section [40–43]. The composition of omphacite was modeled by the diopside–jadeite–hedenbergite-Ca-tschermak system, $CaMgSi_2O_6$-$NaAlSi_2O_6$-$CaFeSi_2O_6$-$CaAl_2SiO_6$. For garnet, the model implying immiscibility between pyrope and grossular at 3 GPa was chosen.

The carbonate solution model was chosen based on the latest data for the $CaCO_3$-$MgCO_3$-$FeCO_3$ system [44–46]. The oCcM(EF) model of Franzolin et al. [37] was the closest of those that contained all three components. The dis(EF) model of Franzolin et al. [37] does not account for the formation of Dol and Ank phases with variable compositions, which is inconsistent with experimental results for binary and ternary carbonates [44–46]. In this regard, the oCcM(EF) model parameters for carbonate solid solutions were adjusted so that the calculated *T-X* diagrams of $CaCO_3$-$MgCO_3$ were as close as possible to the experimentally determined ones [45]. The W parameters of the oCcM(EF) model for the $CaCO_3$-$MgCO_3$ compounds compound were slightly modified in accordance with the experimental results of Shatskiy et al. [45]. The key difference from the original model is the absence of a miscibility gap in the region of compositions with Ca# > 50 near the solidus line, which significantly affects the topology of the diagrams. Modification was made by trial-and-error method. The selected parameters of chemical interaction have the following values: W(Mgs, Cal) = 25,000 J/mol, W(Cal, Dol) = 8200 J/mol, and W(Mgs, Dol) = 15,500 J/mol. In many other parameters, it is still the original oCcM(EF) model.

The LIQ(EF) model is the only carbonate melt model presented in the Perple_X database. It, together with the oCcM(EF) model, is based on the experiments at 3.5 GPa in $CaCO_3$-$MgCO_3$-$FeCO_3$ system [37]. The lack of reliable models simulating mantle carbonatite melts casts doubt on the validity of calculated suprasolidus phase relationships. Therefore, phase fields located above the experimentally inferred solidus of the silicate–CO_2 systems should be considered imaginary. The problem is discussed in detail in the discussion section.

3. Results

3.1. Pyrope–Grossular

In the beginning, we calculated the pyrope–grossular–CO_2 system, which has the greatest deviations from the ideal solution. The results are summarized in the isobaric *T-X* diagrams given in Figure 1. There are more than two phases in the phase fields because the isobaric *T-X* diagrams are pseudo-binary systems.

As can be seen, the Grt+CO_2 fields (shown in dark gray) have a complex shape and occupy limited areas in the *T-X* space. On the pyrope side, the Grt+CO_2 field is much wider than that on the grossular side. Even at 6 GPa, at which the mutual solubility of garnets is not limited, the Grt+CO_2 field does not go beyond Ca#60 on the pyrope side and completely disappears on the grossular side. At higher bulk Ca#, partial melting occurs. Thus, at higher temperatures and Ca#, the formation of a carbonate melt turns out to be thermodynamically more favorable than the transition to the Grt+CO_2 assemblage. It should be noted that the melt model used in the present study does not take into account the possible influence of CO_2 on the melting of the system. See the discussion section for the details.

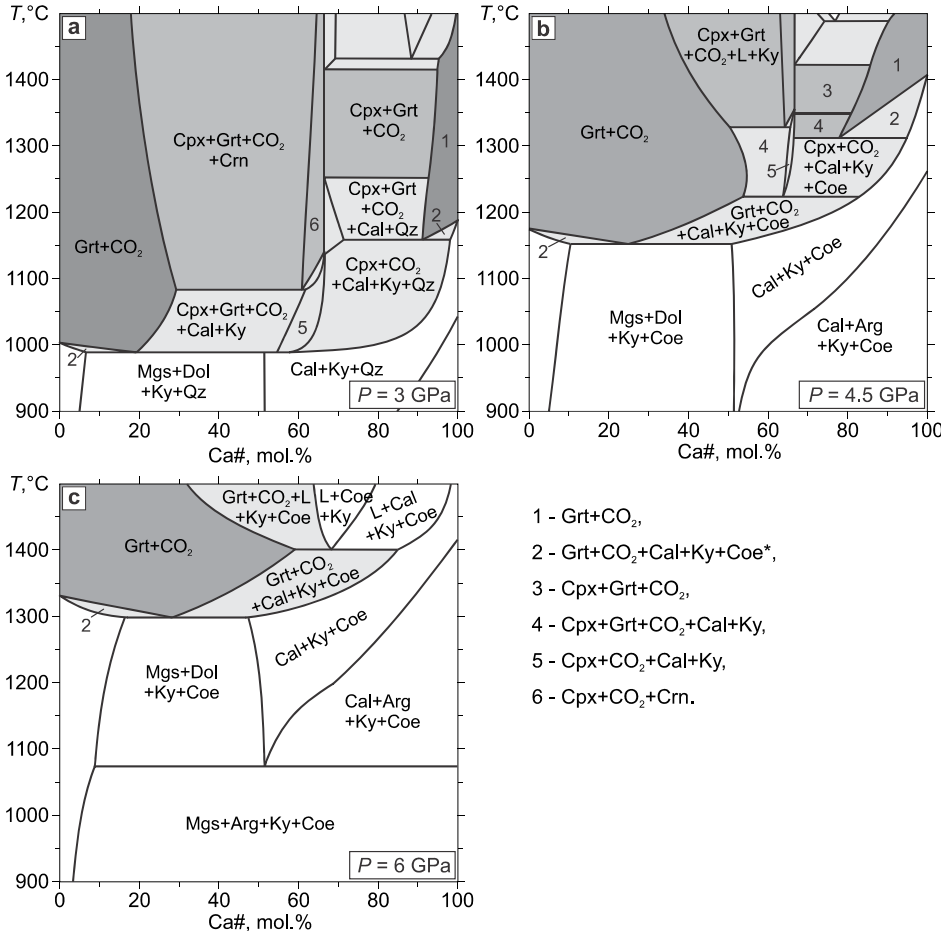

Figure 1. *T-X* diagrams for the pyrope–grossular–CO_2 system at 3 GPa (**a**), 4.5 GPa (**b**), and 6 GPa (**c**). Fields containing CO_2 fluid are highlighted in gray. The garnet–CO_2 fields are highlighted in dark gray. Ca# = Ca/(Ca + Mg) × 100 atomic ratio.

In the low-temperature part of the *T-X* diagrams, the Carb+Ky+Coe fields appear (the unshaded fields in Figure 1). Their shape follows that of the corresponding fields on the $CaCO_3$-$MgCO_3$ *T-X* diagrams. As can be seen, the Carb+Ky+Coe fields do not have a common boundary with the Grt+CO_2 fields, only point contacts at Ca# 0, 20–30, and 100. For the remaining compositions, the Carb+Ky+Coe and Grt+CO_2 fields are separated by the Grt+CO_2+Cal+Ky+Coe/Cpx fields.

The upper part of the *T-X* diagrams (Figure 1a,b) contains regions describing phase equilibria involving silicate melt, garnet, and pyroxene. Since they are not involved in carbonation reactions and have no effect on them, they are not considered in this study and are left unlabeled.

Unlike pyrope, the garnets of the pyrope–grossular series do not react with CO_2 via reaction 1. Figure 2 shows the *P-T* pseudo-sections calculated for Ca# 20, 40, 50, 60, and 80. There is a low-temperature boundary of the Grt+CO_2 field (the orange lines in Figure 2b–f), below which garnet reacts with CO_2 to produce Grt+CO_2+Cal+Ky+Coe and the newly formed garnet has a distinct composition. Moreover, there is a boundary below which the CO_2 fluid completely reacts with the garnet (the blue lines in Figure 2b–f).

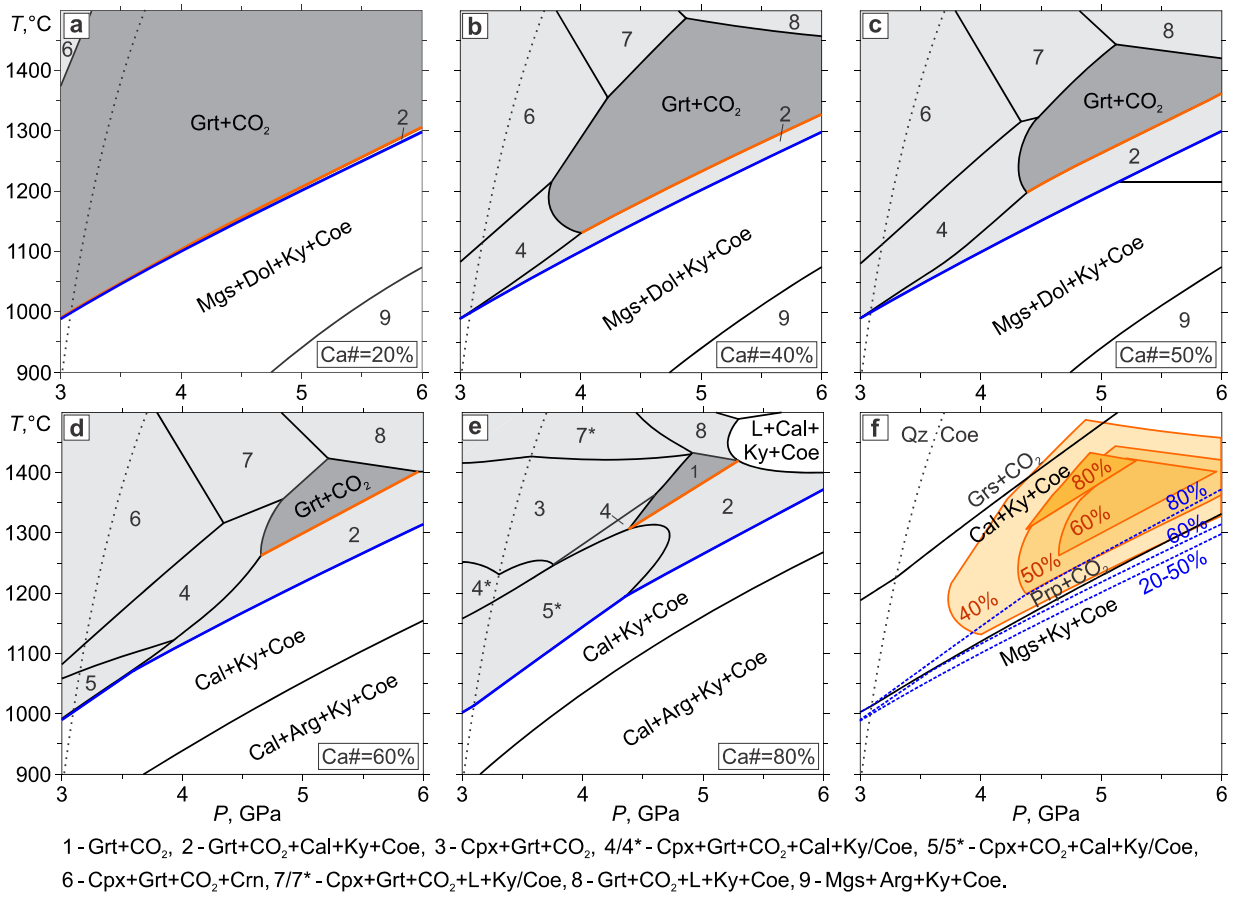

Figure 2. *P-T* diagrams illustrating phase relations in the Prp–Grs–CO_2 system for Ca#: 20 (**a**), 40 (**b**), 50 (**c**), 60 (**d**), and 80 (**e**). The last diagram (**f**) compares phase boundaries at different bulk Ca#. The garnet–CO_2 fields are highlighted in dark grey and orange. Fields of partial carbonation are shaded in light gray.

In the range of Ca# from 20 to 50, the full carbonation line does not change its position and experiences a slight upward shift as the Ca# increases to 60–80 (Figure 2f). At Ca# 20 and less, the lines of partial and full carbonation almost coincide. As the Ca# increases from 20 to 80, the partial carbonation line (orange in Figure 2) shifts upward, widening the region of partial carbonation, which is represented by the Grt+CO_2+Cal+Ky+Coe assemblage (field 2 in Figure 2a–e). Below 4.5 GPa and Ca# > 50, the Grt+CO_2+Cal+Ky+Coe assemblage is replaced with the Cpx+CO_2+Cal+Ky/Coe assemblage (fields 5 and 5* in Figure 2d,e), yielding a change in the clapeyron slope (Figure 2d,e). At lower pressures and higher temperatures, the Cpx+Grt+CO_2+Cal+Ky/Coe assemblage stabilizes (fields 4 and 4* in Figure 2b–e).

3.2. Pyrope–Almandine–Grossular

The calculations were performed for the Prp–$Alm_{50}Grs_{50}$ section, which is the most representative for eclogites (Figure 3). The results of the calculations are shown in Figure 4. As can be seen, the *T-X* space contains three regions: Grt+CO_2, Grt+CO_2+Carb+Ky+Coe (partial carbonation region), and Carb+Ky+Coe (full carbonation region). The last two regions are divided into several fields owing to the diversity of carbonates in the $CaCO_3$-$MgCO_3$-$FeCO_3$ join. The Grt+CO_2 region appears at high temperatures and is continuous over the entire range of compositions. It is separated from the Carb+Ky+Coe region by the Grt+CO_2+Carb+Ky+Coe region (Figure 4a–c). Thus, for the section considered, no garnet would react with CO_2 to produce the Carb+Ky+Coe assemblage directly.

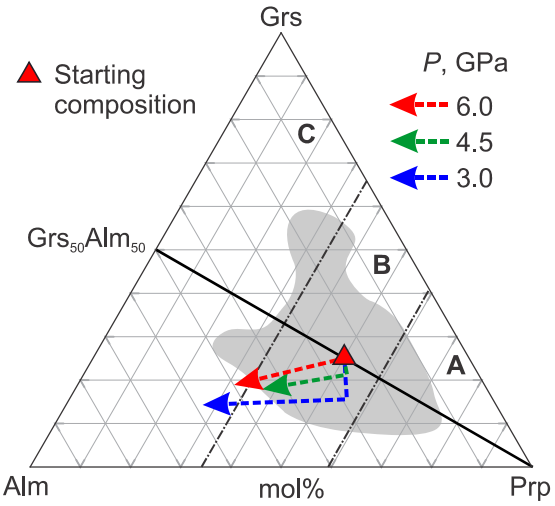

Figure 3. Diagram of the composition of garnets from eclogites [47]. The grey area shows the field of garnets from eclogite xmenoliths from Udachnaya kimberlite pipe (Yakutia, Russia). The eclogitic garnets of Groups A, B, and C according to the classification of Taylor and Neal (Taylor and Neal, 1989). The black solid line shows the cross-section taken to calculate the *T-X* diagrams. The red triangle is the starting composition of $Prp_{50}Grs_{25}Alm_{25}$ garnet. The dotted lines with the arrow show the change in the composition of garnet in the field of partial carbonation with decreasing temperature.

On *T-X* diagrams, the lower boundary of the Grt+CO_2 field (partial carbonation line) extends from the Prp to the $Grs_{50}Alm_{50}$ side through a minimum temperature situated around (Ca+Fe)# 40–50. The maximum variations in temperature at a constant pressure of the partial carbonation line do not exceed 40–80 °C (Figure 4a–c). In contrast, the upper margin of the Carb+Ky+Coe assemblage (full carbonation line) continuously decreases by 200–250 °C along the Prp–$Grs_{50}Alm_{50}$ section. This expands the field of partial carbonation in the direction from the Prp toward the $Grs_{50}Alm_{50}$ (the light-gray area in Figure 4a–c).

For the $Prp_{50}Grs_{25}Alm_{25}$ composition, the *P-T* pseudo-section was calculated (Figure 4d). As can be seen, the lines of partial and full carbonation of the $Prp_{50}Grs_{25}Alm_{25}$ solid solution are lower in temperature than those of the pyrope carbonation line (Prp+CO_2) but higher than those of the almandine carbonation line (Alm+CO_2).

The composition of the garnet in the field of partial carbonation differs from the composition of the garnet in the Grt+CO_2 field, where it corresponds to the bulk composition of the system. The garnet in the partial carbonation field is richer in the almandine component, whose content increases with decreasing temperature (Figure 3).

Our calculations predict an increased CO_2 stability with the three-component garnet due to the almandine component, although it is lower than that of pure almandine. In this case, for all of the garnet compositions in the considered section, a region of partial carbonation is observed, in which the garnet and the carbonate phase coexist (Figure 4a–c). During the partial carbonation, iron and, to a lesser extent, magnesium accumulate in the garnet, while the calcium actively passes into the carbonate phase.

3.3. Eclogite–CO_2

Since at high pressures not only garnet, but also clinopyroxene can react with CO_2, it is of interest to study the garnet–clinopyroxene–CO_2 system to clarify the region of stability of CO_2 in the eclogite mantle. The main components of clinopyroxene in eclogites are diopside and jadeite. An experimental study of the reaction of diopside–jadeite solid solutions with CO_2 showed that the jadeite component does not react with CO_2 up to at least 950 °C at 6 GPa [28]. Therefore, the $CaCO_3$-$MgCO_3$-$FeCO_3$ ternary solid solution model was employed for calculations of the carbonate portion, while the Na_2CO_3 component was ignored. However, at high temperatures, a carbonate melt is formed, which also

contains dissolved Na_2CO_3. Unfortunately, at present, there is no model for such a melt in the Perple_X v. 7.1.3 database. Despite this, it was decided to carry out calculations with existing models of solid solutions to identify the possible interactions between solid phases. To reduce possible distortions due to differences in the composition of the melt, clinopyroxene with a low jadeite content was used for our calculations. Since the previously discussed garnet falls into Group B according to the classification of Taylor and Neal [48], the pyroxene was taken from the same group. An equimolar mixture of $Prp_{50}Grs_{25}Alm_{25}$ garnet and $Di_{70}Jd_{30}$ pyroxene was employed to model the eclogite. CO_2 was added in an amount equal to the number of cations in the system. The composition of the system can be approximated as follows: $Prp_{50}Grs_{25}Alm_{25}$+$Di_{70}Jd_{30}$+5CO_2.

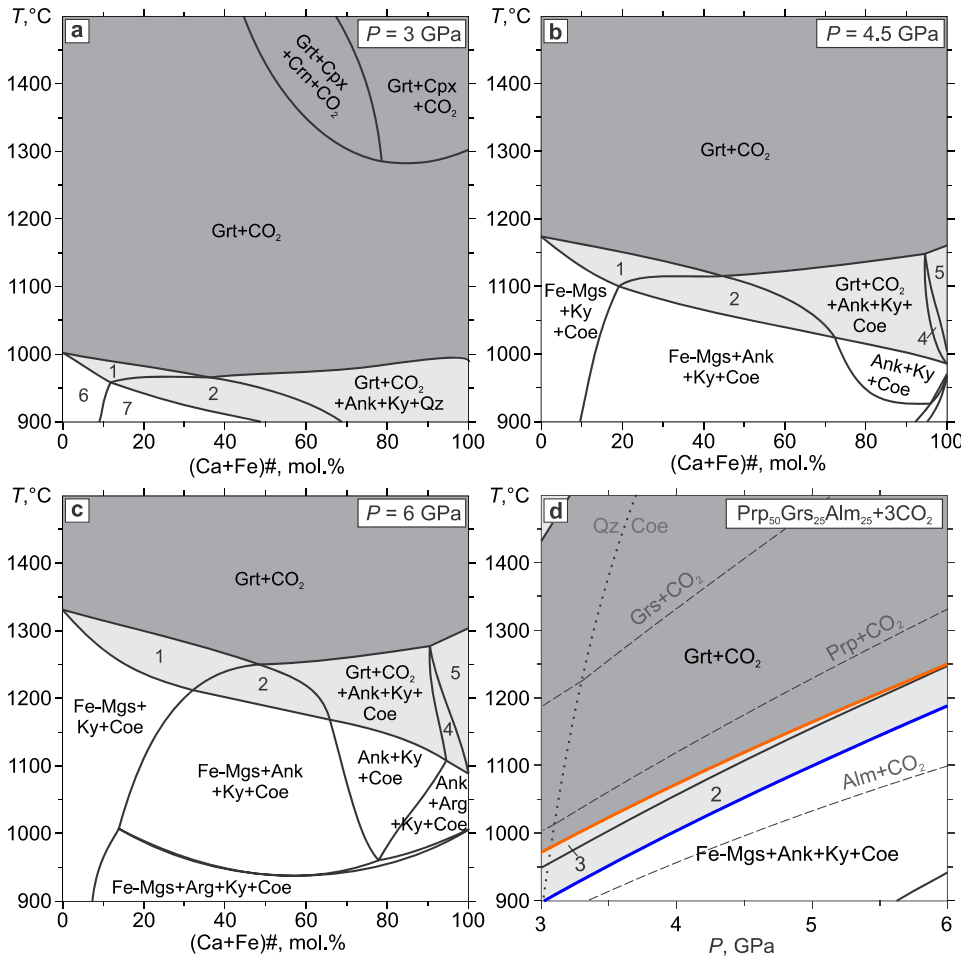

Figure 4. Phase relations in the Prp–$Grs_{50}Alm_{50}$+3CO_2 system. *T-X* diagrams at 3 GPa (**a**), 4.5 GPa (**b**), and 6 GPa (**c**). *P-T* diagram for the $Prp_{50}Grs_{25}Alm_{25}$+3CO_2 bulk composition (**d**). The dotted lines show the equilibrium lines for the reactions of end-member phase components with CO_2. The orange line is the decarbonation reaction. The blue line is the partial decarbonation reaction. The garnet–CO_2 fields are highlighted in dark grey. Fields of partial carbonation are shaded in light gray. Unfilled areas are complete carbonation fields.

As the eclogite carbonates, the clinopyroxene composition shifts to be more jadeitic. The presence of the jadeite component extends the stability range of clinopyroxene to at least 900 °C and 6 GPa (Figure 5a). At these *P-T* conditions, the jadeite component predominates in the clinopyroxene composition. As the temperature increases, the diopside content increases (Figure 6b), even though pure diopside at these conditions is unstable

with CO_2 (Figure 5a). Thus, the Carb+Ky+Coe+Cpx+CO_2 assemblage forms as a result of the full carbonation of eclogite. The clinopyroxene fraction in this assemblage does not exceed 5 mol% (Figure 5b).

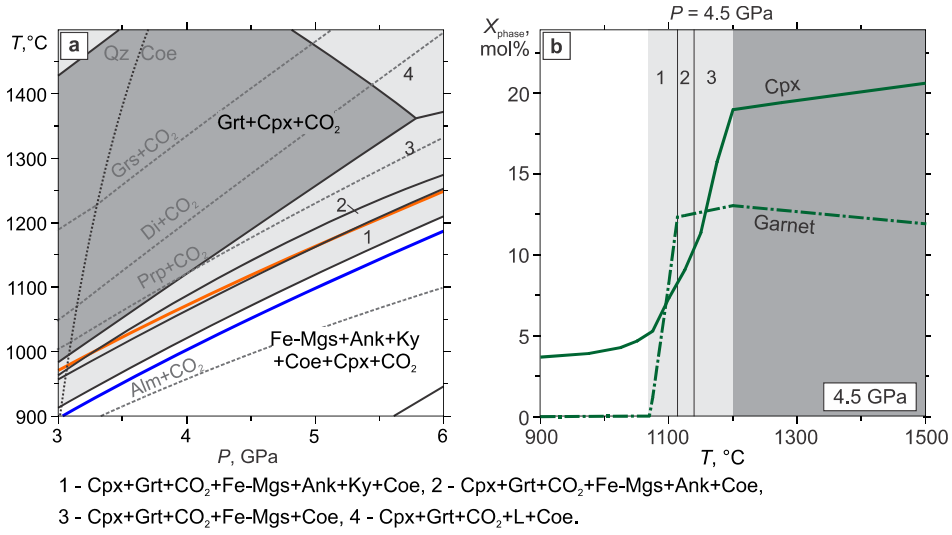

Figure 5. Phase relations in the $Prp_{50}Grs_{25}Alm_{25}$+$Di_{70}Jd_{30}$+5CO_2 system. (**a**) *P*-*T* diagram. The dotted lines show the equilibrium lines for the reactions of end-member phase components with CO_2. The orange line is the partial carbonation line of Prp–$Grs_{50}Alm_{50}$ garnet. The blue line is the carbonation line of Prp–$Grs_{50}Alm_{50}$ garnet. Fields of partial carbonation of garnet are highlighted in gray. The eclogite–CO_2 field is highlighted in dark gray. (**b**) Mole fractions of garnet (dash-dotted line) and clinopyroxene (solid line) as a function of temperature at 4.5 GPa.

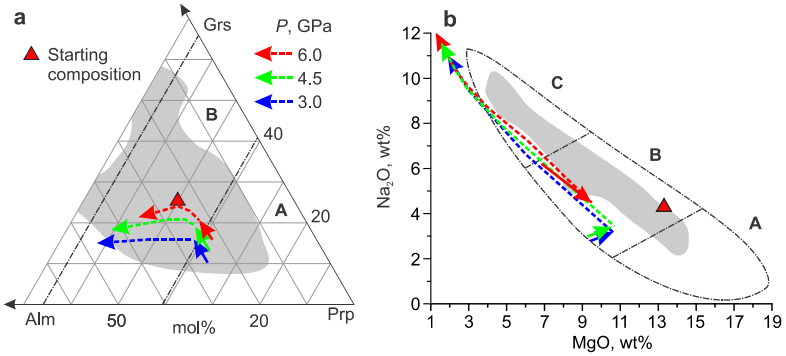

Figure 6. Calculated garnet (**a**) and clinopyroxene (**b**) compositions in the $Prp_{50}Grs_{25}Alm_{25}$+$Di_{70}Jd_{30}$+5CO_2 system at 3, 4.5, and 6 GPa compared with the eclogitic garnet and clinopyroxene of Group A, B, and C, according to the classifications of Coleman et al. [49] and Taylor and Neal [48], respectively. The ranges of eclogitic garnet compositions (light-grey area) and omphacite (light-grey area) correspond to those of Taylor et al. [47]. The dotted and solid lines with the arrow show the change in the composition of garnet (**a**) and clinopyroxene (**b**) in the field of partial carbonation and the eclogite–CO_2 field, respectively, with decreasing temperature. The red triangles are initial compositions of garnet and clinopyroxene.

In the field of the partial carbonation of eclogite, both pyroxene and garnet are present (the light-grey field in Figure 5a). Their fraction increases sharply with increasing temperature (Figure 5b). The region of partial carbonation itself is somewhat wider than that calculated for the $Prp_{50}Grs_{25}Alm_{25}$+3CO_2 system due to the deviation in the upper boundary—the eclogite carbonation line—towards higher temperatures. It can be assumed that these deviations are caused by the reaction of clinopyroxene with CO_2 since garnet has an almost uniform composition and fraction above field 1 (Figures 5b and 6a), which coincides with the carbonation

line of the garnet $Prp_{50}Grs_{25}Alm_{25}$ (Figure 5a). The mole fraction of the garnet in the system shows an inflection during the transition from field 1 to field 2 (Figure 5b).

The composition of garnet in the region of partial carbonation changes from more almandine to more pyrope with increasing temperature. The grossular content increases with pressure and remains almost unchanged with temperature (Figure 6b). The diopside content (MgO/Na_2O ratio) in clinopyroxene increases with increasing temperature. The component ratios shift because of the re-equilibration with garnet, resulting in differences in clinopyroxene compositions at different pressures. The iron content in clinopyroxene remains at approximately the same level of about 4 wt% FeO or 12 mol% hedenbergite.

According to the calculation results, when clinopyroxene and garnet are present together, they react with CO_2 in parallel with the compositions re-equilibrating among themselves. The composition of garnet and clinopyroxene in the Grt+Cpx+CO_2 field is somewhat different from the initially specified one. Garnet contains more pyrope (55–60 mol%) and significantly less grossular (about 15–20 mol%) due to the formation of the Ca-tschermak component in clinopyroxene (Figure 6). The lower margin of the Grt+Cpx+CO_2 field almost coincides with the pyrope carbonation reaction. At 5.7 GPa, it abuts the solidus line of the system (Figure 5a). The line of carbonation of the eclogite lies significantly below the line of the reaction of the diopside with CO_2 due to the presence of hedenbergite in the clinopyroxene composition (Figure 5a).

The lower boundary of the eclogite + CO_2 field intersects the graphite-to-diamond transition line at 4.9 GPa and 1250 °C (Figure 7). As can be seen, the overlap of the Ecl+CO_2 field and *P-T* conditions for the formation of lithospheric diamonds occurs in a very narrow region corresponding to a geotherm of 42 mW/m^2 and depths of ≥160 km. At the same time, the lower boundary of the field of carbonated eclogite + CO_2 crosses the graphite-to-diamond transition near 4.3 GPa and 1050 °C, which corresponds to a heat flow of 39 mW/m^2 (the pink field in Figure 7). At a heat flow of 37 mW/m^2 in the considered pressure range, only the Carb+Ky+Coe+Cpx+CO_2 assemblage is stable (Figure 7).

Since the melt model does not fully describe the melting reaction, the solidus line of the eclogite–CO_2 system from Yaxley and Brey [5] was taken as the upper boundary of the Ecl+CO_2 field (green line in Figure 7). The calculated subsolidus assemblage is represented by Grt+Cpx+Cal-Dol±Coe. At pressures > 5.5 GPa, the calculated solidus (Figure 5a) continues the experimental solidus reported by Yaxley and Brey [5] for the Grt+Cpx+Cal-Dol±Coe assemblage (Figure 7).

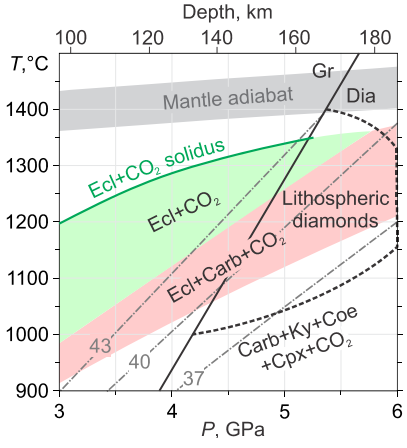

Figure 7. Phase relationships in the system of eclogite–CO_2 according to thermodynamic calculations. The *P-T* fields of CO_2 fluid stability in the eclogitic suite and partial carbonation of eclogite are shown in grey and pink, respectively. The green line is the solidus of the system of eclogite–CO_2 taken from Yaxley and Brey [5]. Gr/Dia—graphite-to-diamond transition [50]. Dash-dotted lines—continental geotherms (37, 40, and 43 mW/m^2) after Hasterok and Chapman [51]. Mantle adiabat (light grey) is taken from [52]. The dotted line delimits the *P-T* range of lithospheric diamond formation.

4. Discussion

The key difference between our results and previously known data is the presence of the so-called region of partial carbonation. In this region, the silicates, CO_2 fluid, carbonates, kyanite, and coesite are in equilibrium. The width of the field of partial carbonation of the eclogite varies from 70 to 150 °C depending on the bulk composition and pressure (Figures 4 and 5). The width of this field is comparable to or exceeds the typical temperature step of multi-anvil experiments (50–100 °C). This means that a similar assemblage should have been observed earlier in experiments. Indeed, in the work of Bataleva et al. [25] on the $Prp_{35}Alm_{40}Grs_{25}$-CO_2 system, the resulting samples contained garnet, carbonates (dolomite, ankerite, Fe–magnesite) kyanite, and coesite. When analyzing the data, the authors of the work proceeded from the results for the pyrope–CO_2 system, for which only two stable assemblages were possible—Prp+CO_2 and Mgs+Ky+Coe. Accordingly, since the starting material was a carbonate–oxide mixture, the appearance of garnet in it was interpreted as a transition to the Grt+CO_2 stability field. According to our calculations, these observations [25,29] should be interpreted as a transition to the Grt+CO_2+Carb+Ky+Coe field. This hypothesis is supported by the small difference in the position of the lines obtained for the Mgs+Ky+Coe and Dol+Ky+Coe mixtures, as well as the nature of the shift in the compositions of the resulting garnets from the initial Ca/Mg/Fe ratio. From the dolomite with $Mgs_{50}Cal_{50}$, the garnet $Prp_{83}Grs_{17}$ was formed, i.e., a more pyrope-rich garnet, while from the ankerite $Mgs_{37}Cal_{47}Sid_{15}$ $Prp_{35}Grs_{25}Alm_{40}$ was formed, i.e., a more ferrous garnet with less calcium. Similar compositional shifts were observed in the region of partial carbonation. In addition, according to our calculations, in this region, the composition of the garnet depends on the pressure, which was also observed in the work of Bataleva et al. [25].

According to our calculations, for a Grt–CO_2 system with the same bulk composition, the carbonation and decarbonation lines do not coincide. This is an important feature of the CO_2 reaction with the Prp–Alm–Grs solid solution since the Grt+CO_2 and Carb+Ky+Coe fields are separated by the Grt+CO_2+Carb+Ky+Coe field.

Although thermodynamic calculations were used in all previous works [23,25,29], their results did not reveal the presence of a region of partial carbonation. This discrepancy is caused by the difference in approaches for calculating reactions of solid solutions. The earlier studies employed a fixed composition of the solid solution, specified through the values of the activities of the components. Knoche et al. [23] and Vinogradova et al. [30] calculated lines for each of the components, taking into account the changed activity using the TWQ program of Berman [53] version 1.02, JUN92.GSC mineral data, and the THERMOCALC program of Holland and Powell [36] version 3.45, respectively. Bataleva et al. [25] calculated the general position of the reaction line using the approach reported in [53,54], but the reaction is generated based on the reaction equations of the end-member phase components. Therefore, both algorithms do not imply the possibility of forming a stable assemblage other than Carb+Ky+Coe and Grt+CO_2.

The Perple_X v. 7.1.3 software package differs in that the user specifies the bulk composition of the system, and then the algorithms generate a set of possible solid solutions with a certain compositional step. From the resulting set of phases, the thermodynamically most favorable assemblage at a specific point in the diagram is identified. Thus, the program calculates the phase composition over the entire field of the diagram with a given grid and then adds boundaries between points of different compositions. With this approach, the reaction equations of the end-member phase components and their solutions do not appear in any way in the calculations, but they are determined later based on the results. Only the boundaries of the phase transitions between different polymorphs of the same substance are fixed.

The result of calculations in Perple_X v. 7.1.3 is strongly influenced by the list of solution models that the user selects. For example, if we exclude the clinopyroxene model when calculating the Prp–Grs-CO_2 diagram (Figure 2), the result will show a continuous solution for the garnet at all pressures, as was the case in the Prp–Grs–Alm–CO_2 system

(Figure 4). The area of partial carbonation will remain. The rationale for our choice of specific solution models is outlined in the methods section. Here, it should be noted that the existing solution database for Perple_X v. 7.1.3 contains very few models for carbonate melts. The LIQ(EF) model we chose is the only one suitable for the Ca-Mg-Fe carbonate melt but it does not take into account the presence of sodium and the possible dissolution of molecular CO_2.

For Ca and Mg carbonates, it has been experimentally shown that CO_2 will dissolve in the carbonate melt, and its solubility increases with increasing pressure [55]. In this case, the melting point of the carbonate–CO_2 mixture is lower than that of the original carbonate. A similar effect can be expected in the system we are studying in the current paper, especially for the areas for which the program predicts the coexistence of CO_2 and carbonate melts. This assumption is confirmed by the results of experiments in Di-CO_2 and Di–Jd–CO_2 systems [26,28], which showed a decrease in the melting temperature compared to carbonate–silicate systems without an excess of CO_2 [56]. In addition, the Di–Jd–CO_2 system has a lower melting point compared to that of diopside–CO_2.

In addition, the CO_2 fluid itself can act as a solvent, as evidenced by the experimental results presented in the article by Novoselov et al. [31]. According to the authors, CO_2 partially dissolves garnet in the absence of carbonation, and predominantly Ca passes into the fluid. This process, firstly, will change the composition of garnet even within the Grt+CO_2 region, and secondly, it will reduce the activity of CO_2 itself, which will affect the position of the region boundaries on phase diagrams.

Summarizing the above, we can conclude that diagrams for real systems may have a slightly different position of the boundaries, different from the calculated one, due to possible phase mixing that is not taken into account by the models. Since it seems extremely difficult to take into account all of these effects in calculations, it is necessary to conduct an experimental study of the phase relationships in the garnet–CO_2 and eclogite–CO_2 systems, taking into account the discovered features.

Due to clinopyroxene, the temperature of the onset of carbonation of eclogite is significantly higher than that of garnet, which shifts the eclogite + CO_2 field in the *P-T* stability field of diamond to temperatures exceeding 1250 °C (Figure 7). Although the eclogite–carbonate–CO_2 assemblage is stable at lower temperatures, under conditions of CO_2 deficiency, the CO_2 fluid will be completely consumed for the eclogite carbonation just below the eclogite + CO_2 field stability.

CO_2 fluid is stable under oxidized conditions corresponding to the CCO buffer. Sokol et al. [57,58] performed the chromatographic analysis of the C-O-H fluid coexisting with graphite/diamond under reduced conditions controlled by an Fe-FeO buffer, which was quenched at 5.7–6.3 GPa and 1200–1600 °C. Their results show that the quenched fluid varies from H_2O >> H_2 > CH_4 (at fO_2 value somewhat lower than the "water maximum") to H_2 > CH_4 > (C_2H_4 + C_2H_6) > C_3H_8 (in the C–H system). These experiments indicate that the sequential reduction in CO_2-bearing fluid yields the precipitation of diamond and changes the fluid composition to H_2- and CH_4-bearing H_2O and finally to CH_4-H_2 fluid. This agrees well with the Raman spectra from the Fe-Ni-C-S melt inclusions in large gem diamonds, which revealed the presence of methane and hydrogen [59]. Thus, diamond, Fe-Ni-S-C melt, and methane are the main carbon hosts in the mantle under reduced conditions, while CO does not form under a high pressure.

Findings of CO_2 fluid in diamonds [20,21] may not be accidental. CO_2 fluid can be formed as a result of the metamorphic degassing of oceanic plates when they are heated during low-angle subduction beneath the continental lithospheric mantle [7,60,61]. It was experimentally shown that CO_2 fluid could be responsible for diamond crystallization as a solvent catalyst [62,63] and carbon source [64]. Most of the mineral inclusions found in CO_2-bearing diamonds belong to the eclogitic suite [13,20,21]. Indeed, our results show that, in contrast to ultramafic rocks, CO_2 fluid could be stable in the eclogitic suite under *P-T* conditions of lithospheric diamond formation at temperatures exceeding 1250 °C (Figure 7). The penetration of CO_2 fluid into the eclogitic mantle should be accompanied by partial

carbonation, a decrease in the pyrope component in garnet, and an increase in the jadeite component in clinopyroxene, shifting the composition of the eclogite towards Group C.

5. Conclusions

Based on the results of our thermodynamic calculations in the Perple_X v. 7.1.3 software package for the systems of Prp–Grs+3CO_2, Prp–$Alm_{50}Grs_{50}$+3CO_2, and $Prp_{50}Grs_{25}Alm_{25}$+$Di_{70}Jd_{30}$+5CO_2 conducted using the ranges of 3–6 GPa and 900–1500 °C, the following conclusions can be drawn:

(1) In the Prp–Grs+3CO_2 system, from the low-pressure and high-temperature side, the Grt+CO_2 field is limited by the reaction of the partial decomposition of garnet:

$$\mathrm{Grt} \rightarrow \mathrm{Cpx} \pm \mathrm{Grt_{new}} \pm \mathrm{Crn}. \quad (2)$$

On the high-pressure and low-temperature side, the Grt+CO_2 field is restricted by the reaction of the partial carbonation of garnet:

$$\mathrm{Grt} + 3\mathrm{CO_2} \rightarrow \mathrm{Grt_{new}} + \mathrm{CO_2} + \mathrm{Cal} + \mathrm{Ky} + \mathrm{Coe}. \quad (3)$$

On the low-pressure and low-temperature side, the field Grt+CO_2 is limited by the combination of reactions 2 and 3. On the high-pressure and high-temperature side, the field Grt+CO_2 is restricted by the system solidus and the formation of a carbonate melt. We also expect that adding water, which generally lowers the solidus, should restrict the CO_2 fluid stability field. At Ca# of 20–30, the reaction lines of the partial and full carbonation of the grant are almost identical. As the Ca# of the system increases above 30, the lower boundary of the Grt+CO_2 field shifts towards low pressures and high temperatures. However, because the full carbonation line hardly changes its position, the area where garnet can coexist with CO_2 remains almost unchanged when the Ca# changes from 20 to 80.

(2) The addition of almandine to the Prp–Grs+CO_2 system shifts the limit of partial carbonation of garnet by 30–70 °C and the full carbonation of garnet by 100–140 °C below the Prp+CO_2 line. The Grt+CO_2 region appears at high temperatures and is continuous over the entire range of compositions. Along the Prp–$Alm_{50}Grs_{50}$ join, there is no garnet composition that would react with CO_2 to produce the Carb+Ky+Coe assemblage directly. The regions of Grt+CO_2 and Carb+Ky+Coe are separated by the Grt+CO_2+Carb+Ky+Coe field. The composition of garnet in the field of partial carbonation is richer in the almandine component than that in the Grt+CO_2 field.

(3) In the eclogite–CO_2 system, the lower boundary of the Grt+Cpx+CO_2 assemblage almost coincides with the pyrope carbonation reaction. In the field of partial carbonation, the garnet and omphacite react with CO_2 to form carbonate, kyanite, coesite, garnet, and clinopyroxene with a new composition. Due to the carbonation of clinopyroxene, the temperature of the partial carbonation of eclogite is significantly higher than that of garnet, which restricts the eclogite + CO_2 stability field to pressures lower than the diamond stability field. The partial carbonation of the eclogite stabilizes the carbonate, kyanite, and coesite, wherein, the garnet composition shifts toward more almandine, while the clinopyroxene composition evolves to jadeite. This would extend the CO_2 stability field in the eclogitic suite to lower temperatures. Yet, taking into account the fact that CO_2 is in short supply under natural conditions, it should be completely spent on the carbonation of the eclogite just below the eclogite + CO_2 field.

Author Contributions: Conceptualization, A.S. and Y.G.V.; methodology, Y.G.V.; software, Y.G.V.; validation, Y.G.V.; formal analysis, Y.G.V.; investigation, Y.G.V.; resources, A.S.; data curation, Y.G.V.; writing—original draft preparation, Y.G.V.; writing—review and editing, A.S.; visualization, Y.G.V. and A.S.; supervision, A.S.; project administration, A.S.; funding acquisition, A.S. All authors have read and agreed to the published version of the manuscript.

Funding: This research was funded by the Russian Science Foundation (project No 21-77-10057).

Data Availability Statement: Not applicable.

Acknowledgments: We are grateful to the three anonymous reviewers and to our academic editor for their comments, which helped to improve the manuscript.

Conflicts of Interest: The authors declare no conflicts of interest.

Abbreviations

Ank	ankerite
Alm	almandine
Arg	aragonite
Cal	calcite
Carb	carbonate
Coe	coesite
Cpx	clinopyroxene
Crn	corundum
Di	diopside
Dol	dolomite
Ecl	eclogite
Grs	grossular
Grt	garnet
Jd	jadeite
Ky	kyanite
Mgs	magnesite
Qz	quartz
Prp	pyrope

References

1. Wyllie, P.J.; Huang, W.L. Inflence of mantle CO_2 ingeneration of carbonatites and kimberlites. *Nature* **1975**, *257*, 297–299. [CrossRef]
2. Kerrick, D.M.; Connolly, J.A.D. Metamorphic devolatilization of subducted marine sediments and the transport of volatiles into the Earth's mantle. *Nature* **2001**, *411*, 293–296. [CrossRef] [PubMed]
3. Kerrick, D.M.; Connolly, J.A.D. Metamorphic devolatilization of subducted oceanic metabasalts: Implications for seismicity, arc magmatism and volatile recycling. *Earth Planet. Sci. Lett.* **2001**, *189*, 19–29. [CrossRef]
4. Yaxley, G.M.; Green, D.H. Experimental demonstration of refractory carbonate-bearing eclogite and siliceous melt in the subduction regime. *Earth Planet. Sci. Lett.* **1994**, *128*, 313–325. [CrossRef]
5. Yaxley, G.M.; Brey, G.P. Phase relations of carbonate-bearing eclogite assemblages from 2.5 to 5.5 GPa: Implications for petrogenesis of carbonatites. *Contrib. Mineral. Petrol.* **2004**, *146*, 606–619. [CrossRef]
6. Dasgupta, R.; Hirschmann, M.M.; Withers, A.C. Deep global cycling of carbon constrained by the solidus of anhydrous, carbonated eclogite under upper mantle conditions. *Earth Planet. Sci. Lett.* **2004**, *227*, 73–85. [CrossRef]
7. Shatskiy, A.; Arefiev, A.V.; Podborodnikov, I.V.; Litasov, K.D. Origin of K-rich diamond-forming immiscible melts and CO_2 fluid via partial melting of carbonated pelites at a depth of 180-200 km. *Gondwana Res.* **2019**, *75*, 154–171. [CrossRef]
8. Shatsky, V.; Ragozin, A.; Zedgenizov, D.; Mityukhin, S. Evidence for multistage evolution in a xenolith of diamond-bearing eclogite from the Udachnaya kimberlite pipe. *Lithos* **2008**, *105*, 289–300. [CrossRef]
9. Zedgenizov, D.A.; Ragozin, A.L.; Shatsky, V.S.; Griffin, W.L. Diamond formation during metasomatism of mantle eclogite by chloride-carbonate melt. *Contrib. Mineral. Petrol.* **2018**, *173*, 84. [CrossRef]
10. Roedder, E. Liquid CO_2 inclusions in olivine-bearing nodules and phenocrysts from basalts. *Am. Mineral. J. Earth Planet. Mater.* **1965**, *50*, 1746–1782.
11. Kennedy, G.C.; Nordlie, B.E. The genesis of diamond deposits. *Econ. Geol.* **1968**, *63*, 495–503. [CrossRef]
12. Schrauder, M.; Navon, O. Solid carbon dioxide in natural diamond. *Nature* **1993**, *365*, 42–44. [CrossRef]
13. Chinn, I.L. A Study of Unusual Diamonds from the George Creek K1 Kimberlite Dyke, Colorado. Ph.D. Thesis, University of Cape Town, Cape Town, South Africa, 1995.
14. Barannik, E.P.; Shiryaev, A.A.; Hainschwang, T. Shift of CO_2-I absorption bands in diamond: A pressure or compositional effect? A FTIR mapping study. *Diam. Relat. Mater.* **2021**, *113*, 108280. [CrossRef]
15. Tomilenko, A.A.; Ragozin, A.L.; Shatskii, V.S.; Shebanin, A.P. Variation in the fluid phase composition in the process of natural diamond crystallization. *Dokl. Earth Sci.* **2001**, *379*, 571–574.

16. Smith, E.M.; Kopylova, M.G.; Frezzotti, M.L.; Afanasiev, V.P. Fluid inclusions in Ebelyakh diamonds: Evidence of CO_2 liberation in eclogite and the effect of H_2O on diamond habit. *Lithos* **2015**, *216*, 106–117. [CrossRef]
17. Pal'yanov, Y.N.; Sokol, A.G.; Khokhryakov, A.F.; Sobolev, N.V. Experimental study of interaction in the CO_2-C system at mantle *PT* parameters. *Dokl. Earth Sci.* **2010**, *435*, 1492–1495. [CrossRef]
18. Wyllie, P.J.; Huang, W. Peridotite, kimberlite, and carbonatite explained in the system CaO-MgO-SiO_2-CO_2. *Geology* **1975**, *3*, 621–624. [CrossRef]
19. Koziol, A.M.; Newton, R.C. Experimental determination of the reaction: Magnesite + enstatite = forsterite + CO_2 in the ranges 6–25 kbar and 700–1100 °C. *Am. Mineral.* **1998**, *83*, 213–219. [CrossRef]
20. Ragozin, A.L.; Shatsky, V.S.; Rylov, G.M.; Goryainov, S.V. Coesite inclusions in rounded diamonds from placers of the Northeastern Siberian Platform. *Dokl. Earth Sci.* **2002**, *384*, 385–389.
21. Ragozin, A.L.; Shatskii, V.S.; Zedgenizov, D.A. New data on the growth environment of diamonds of the variety V from placers of the Northeastern Siberian platform. *Dokl. Earth Sci.* **2009**, *425*, 436–440. [CrossRef]
22. Rohrbach, A.; Schmidt, M.W. Redox freezing and melting in the Earth's deep mantle resulting from carbon-iron redox coupling. *Nature* **2011**, *472*, 209–212. [CrossRef] [PubMed]
23. Knoche, R.; Sweeney, R.J.; Luth, R.W. Carbonation and decarbonation of eclogites: The role of garnet. *Contrib. Mineral. Petrol.* **1999**, *135*, 332–339. [CrossRef]
24. Luth, R.W. Experimental study of the $CaMgSi_2O_6$-CO_2 system at 3–8 GPa. *Contrib. Mineral. Petrol.* **2006**, *151*, 141–157. [CrossRef]
25. Bataleva, Y.V.; Novoselov, I.D.; Kruk, A.N.; Furman, O.V.; Reutsky, V.N.; Palyanov, Y.N. Experimental modeling of decarbonation reactions resulting in Mg, Fe-garnets and CO_2 fluid at the mantle P–T parameters. *Russ. Geol. Geophys.* **2020**, *61*, 650–662. [CrossRef]
26. Shatskiy, A.; Vinogradova, Y.G.; Arefiev, A.V.; Litasov, K.D. Revision of the $CaMgSi_2O_6-CO_2$ *P-T* phase diagram at 3–6 GPa. *Am. Mineral.* **2023**, *108*, 2338–2347. [CrossRef]
27. Vinogradova, Y.G.; Shatskiy, A.; Arefiev, A.V.; Litasov, K.D. The equilibrium boundary of the reaction $Mg_3Al_2Si_3O_{12} + 3CO_2 = Al_2SiO_5 + 2SiO_2 + 3MgCO_3$ at 3–6 GPa. *Am. Mineral.* **2024**, *109*, 384–391. [CrossRef]
28. Shatskiy, A.; Vinogradova, Y.G.; Arefiev, A.V.; Litasov, K.D. The system $NaAlSi_2O_6$–$CaMgSi_2O_6-CO_2$ at 3–6.5 GPa: Implications for CO_2 stability in the eclogitic suite at depths of 100–200 km. *Contrib. Mineral. Petrol.* **2023**, *178*, 22. [CrossRef]
29. Bataleva, Y.V.; Kruk, A.N.; Novoselov, I.D.; Furman, O.V.; Palyanov, Y.N. Decarbonation reactions involving ankerite and dolomite under upper mantle P, T-parameters: Experimental modeling. *Minerals* **2020**, *10*, 715. [CrossRef]
30. Vinogradova, Y.G.; Shatskiy, A.F.; Litasov, K.D. Thermodynamic analysis of the reactions of CO_2-fluid with garnets and clinopyroxenes at 3–6 GPa. *Geochem. Int.* **2021**, *59*, 851–857. [CrossRef]
31. Novoselov, I.D.; Palyanov, Y.N.; Bataleva, Y.V. Experimental modeling of the interaction between garnets of mantle parageneses and CO_2 fluid at 6.3 GPa and 950–1550 °C. *Russ. Geol. Geophys.* **2023**, *64*, 379–393. [CrossRef]
32. Connolly, J.A.D. The geodynamic equation of state: What and how. *Geochem. Geophys. Geosystems* **2009**, *10*, Q10014. [CrossRef]
33. Connolly, J. Computation of phase equilibria by linear programming: A tool for geodynamic modeling and its application to subduction zone decarbonation. *Earth Planet. Sci. Lett.* **2005**, *236*, 524–541. [CrossRef]
34. Holland, T.J.B.; Powell, R. An improved and extended internally consistent thermodynamic dataset for phases of petrological interest, involving a new equation of state for solids. *J. Metamorph. Geol.* **2011**, *29*, 333–383. [CrossRef]
35. Holland, T.J.B.; Green, E.C.R.; Powell, R. Melting of peridotites through to granites: A simple thermodynamic model in the system KNCFMASHTOCr. *J. Petrol.* **2018**, *59*, 881–900. [CrossRef]
36. Holland, T.J.B.; Powell, R.T.J.B. An internally consistent thermodynamic data set for phases of petrological interest. *J. Metamorph. Geol.* **1998**, *16*, 309–343. [CrossRef]
37. Franzolin, E.; Schmidt, M.W.; Poli, S. Ternary Ca–Fe–Mg carbonates: Subsolidus phase relations at 3.5 GPa and a thermodynamic solid solution model including order/disorder. *Contrib. Mineral. Petrol.* **2011**, *161*, 213–227. [CrossRef]
38. Holland, T.; Powell, R. A Compensated-Redlich-Kwong (CORK) equation for volumes and fugacities of CO_2 and H_2O in the range 1 bar to 50 kbar and 100–1600 °C. *Contrib. Mineral. Petrol.* **1991**, *109*, 265–273. [CrossRef]
39. Boyd, F.R. Garnet peridotites and the system $CaSiO_3$-$MgSiO_3$-Al_2O_3. *Mineral. Soc. Amer. Spec. Pap.* **1970**, *3*, 63–75.
40. Maaloe, S.; Wyllie, P.J. Join grossularite-pyrope at 30 kb and its petrological significance. *Am. J. Sci.* **1979**, *279*, 288–301. [CrossRef]
41. Sekine, T.; Wyllie, P.J. Phase relationships in the join grossularite-pyrope 7.5 persent H_2O at 30 kb. *Am. J. Sci.* **1983**, *283*, 435–453. [CrossRef]
42. Surkov, N.V.; Gartvich, Y.G. Experimental study of phase equilibria in the pyrope-grossular join at a pressure of 30 kbar. *Petrology* **2000**, *8*, 84–95.
43. Orlando, A.; Borrini, D. Synthesis of pyrope-grossular garnets: An experimental study at P = 2.5 GPa. *Mineral. Petrol.* **2003**, *78*, 37–51. [CrossRef]
44. Shatskiy, A.; Borzdov, Y.M.; Litasov, K.D.; Kupriyanov, I.N.; Ohtani, E.; Palyanov, Y.N. Phase relations in the system $FeCO_3$-$CaCO_3$ at 6 GPa and 900–1700 °C and its relation to the system $CaCO_3$-$FeCO_3$-$MgCO_3$. *Am. Mineral.* **2014**, *99*, 773–785. [CrossRef]
45. Shatskiy, A.; Podborodnikov, I.V.; Arefiev, A.V.; Minin, D.A.; Chanyshev, A.D.; Litasov, K.D. Revision of the $CaCO_3$–$MgCO_3$ phase diagram at 3 and 6 GPa. *Am. Mineral.* **2018**, *103*, 441–452. [CrossRef]
46. Shatskiy, A.; Litasov, K.D.; Ohtani, E.; Borzdov, Y.M.; Khmelnikov, A.I.; Palyanov, Y.N. Phase relations in the K_2CO_3-$FeCO_3$ and $MgCO_3$-$FeCO_3$ systems at 6 GPa and 900–1700 °C. *Eur. J. Mineral.* **2015**, *27*, 487–499. [CrossRef]

47. Taylor, L.A.; Snyder, G.A.; Keller, R.; Remley, D.A.; Anand, M.; Wiesli, R.; Valley, J.; Sobolev, N.V. Petrogenesis of group A eclogites and websterites: Evidence from the Obnazhennaya kimberlite, Yakutia. *Contrib. Mineral. Petrol.* **2003**, *145*, 424–443. [CrossRef]
48. Taylor, L.A.; Neal, C.R. Eclogites with oceanic crustal and mantle signatures from the Bellsbank kimberlite, South Africa, Part I: Mineralogy, petrography, and whole rock chemistry. *J. Geol.* **1989**, *97*, 551–567. [CrossRef]
49. Coleman, R.G.; Lee, D.E.; Beatty, L.B.; Brannock, W.W. Eclogites and eclogites: Their differences and similarities. *Geol. Soc. Am. Bull.* **1965**, *76*, 483–508. [CrossRef]
50. Day, H.W. A revised diamond-graphite transition curve. *Am. Mineral.* **2012**, *97*, 52–62. [CrossRef]
51. Hasterok, D.; Chapman, D.S. Heat production and geotherms for the continental lithosphere. *Earth Planet. Sci. Lett.* **2011**, *307*, 59–70. [CrossRef]
52. Katsura, T. A revised adiabatic temperature profile for the mantle. *J. Geophys. Res. Solid Earth* **2022**, *127*, e2021JB023562. [CrossRef]
53. Berman, R.G. Thermobarometry using multi-equilibrium calculations: A new technique with petrological application. *Can. Mineral.* **1991**, *29*, 833–855.
54. Ogasawara, Y.; Liou, J.G.; Zhang, R.Y. Thermochemical calculation of log fO_2–T–P stability relations of diamond-bearing assemblages in the model system CaO–MgO–SiO_2–CO_2–H_2O. *Russ. Geol. Geophys.* **1997**, *2*, 587–598.
55. Huang, W.L.; Wyllie, P.J. Melting relationships in the systems CaO-CO_2 and MgO-CO_2 to 33 kilobars. *Geochim. Cosmochim. Acta* **1976**, *40*, 129–132.
56. Dalton, J.A.; Presnall, D.C. Carbonatitic melts along the solidus of model lherzolite in the system CaO-MgO-Al_2O_3-SiO_2-CO_2 from 3 to 7 GPa. *Contrib. Mineral. Petrol.* **1998**, *131*, 123–135. [CrossRef]
57. Sokol, A.G.; Palyanova, G.A.; Palyanov, Y.N.; Tomilenko, A.A.; Melenevsky, V.N. Fluid regime and diamond formation in the reduced mantle: Experimental constraints. *Geochim. Et Cosmochim. Acta* **2009**, *73*, 5820–5834. [CrossRef]
58. Sokol, A.G.; Pal'yanov, Y.N.; Pal'yanova, G.A.; Tomilenko, A.A. Diamond crystallization in fluid and carbonate-fluid systems under mantle P-T conditions: 1. Fluid composition. *Geochem. Int.* **2004**, *42*, 830–838.
59. Smith, E.M.; Shirey, S.B.; Nestola, F.; Bullock, E.S.; Wang, J.; Richardson, S.H.; Wang, W. Large gem diamonds from metallic liquid in Earth's deep mantle. *Science* **2016**, *354*, 1403–1405. [CrossRef] [PubMed]
60. Shatskiy, A.; Arefiev, A.V.; Podborodnikov, I.V.; Litasov, K.D. Liquid immiscibility and phase relations in the join $KAlSi_3O_8$–$CaMg(CO_3)_2$ ± $NaAlSi_2O_6$ ± Na_2CO_3 at 6 GPa: Implications for diamond-forming melts. *Chem. Geol.* **2020**, *550*, 119701. [CrossRef]
61. Shatskiy, A.; Arefiev, A.V.; Podborodnikov, I.V.; Litasov, K.D. Effect of water on carbonate-silicate liquid immiscibility in the system $KAlSi_3O_8$–$CaMgSi_2O_6$–$NaAlSi_2O_6$–$CaMg(CO_3)_2$ at 6 GPa: Implications for diamond-forming melts. *Am. Mineral.* **2021**, *106*, 165–173. [CrossRef]
62. Pal'yanov, Y.N.; Sokol, A.G.; Khokhryakov, A.F.; Pal'yanova, G.A.; Borzdov, Y.M.; Sobolev, N.V. Diamond and graphite crystallization in COH fluid at *PT* parameters of the natural diamond formation. *Dokl. Earth Sci.* **2000**, *375*, 1395–1398.
63. Sokol, A.G.; Pal'yanov, Y.N.; Pal'yanova, G.A.; Khokhryakov, A.F.; Borzdov, Y.M. Diamond and graphite crystallization from C-O-H fluids under high pressure and high temperature conditions. *Diam. Relat. Mater.* **2001**, *10*, 2131–2136. [CrossRef]
64. Bataleva, Y.V.; Palyanov, Y.N. Diamond formation via carbonate or CO_2 reduction under pressures and temperatures of the lithospheric mantle: Review of experimental data. *Minerals* **2023**, *13*, 940. [CrossRef]